

Positron-atom scattering using pseudo-state energy shifts

J.Mitroy* and J.Y.Zhang

*ARC Center for Anti-Matter Studies, Faculty of Technology,
Charles Darwin University, Darwin NT 0909, Australia*

M.W.J.Bromley† and S.I.Young

*Department of Physics and Computational Science Research Center,
San Diego State University, San Diego CA 92182, USA*

(Dated: November 17, 2021)

A method to generate low-energy phase shifts for elastic scattering using bound-state calculations is applied to the problem of e^+ -Mg and e^+ -Zn scattering after an initial validation on the e^+ -Cu system. The energy shift between a small reference calculation and the largest possible configuration interaction calculation of the lowest energy pseudo-state is used to tune a semi-empirical optical potential. The potential was further fine-tuned by utilizing the energy of the second lowest pseudo-state. The s - and p -wave phase shifts for positron scattering from Mg and Zn are given from threshold to the first excitation threshold. The e^+ -Mg cross section has a prominent p -wave shape resonance at an energy of about 0.096 eV with a width of 0.106 eV. The peak cross section for e^+ -Mg scattering is about $4800 a_0^2$ while Z_{eff} achieves a value of 1310 at an energy of 0.109 eV.

PACS numbers: 34.80.Uv, 34.80.Bm, 31.15.A-, 03.65.Nk

One of the most technically demanding problems in quantum physics is the scattering problem, i.e. the prediction of the reaction probabilities when two objects collide [1]. The underlying difficulty lies in the unbounded nature of the wave function. This leads to a variety of computational and analytic complications that are absent in bound state calculations, e.g. the Schwartz singularities that occur in the Kohn variational method for scattering [2, 3].

One approach to solve scattering problems is to use methods that have been used for bound state calculations [1, 4, 5]. There are many examples of such approaches, one of the most popular being the R -matrix methods that use the solutions of the Schrödinger equation in a finite sized cavity to determine the behavior of the wave function in the interaction region [1, 6, 7, 8]. The total wave function is constructed by splicing the inner wave function onto the asymptotic wave function.

This article had its origin in a particular scattering problem, namely the determination of the near threshold phase shifts for positron scattering from the di-valent group II and IIB atoms. The dimension of the secular equations for bound state calculations on such systems are very large, for example a configuration interaction (CI) calculation of the e^+ Ca $^2P^o$ state resulted in equations of dimension 874,448 [9]. These dimensions are much larger than those that would occur in a CI calculation of the $^2P^o$ ground state Ca $^-$. The exceptionally large dimensionalities occur because the valence electrons tend to localize around the positron, thus giving a very slowly convergent partial wave expansion of the wave function

[10, 11, 12, 13, 14, 15]. The ability to routinely solve the secular equations associated with the CI basis using iterative sparse matrix techniques [16] is one reason why CI calculations for positronic atoms (and of course for molecular systems) have been able to generate useful results.

Trying to generate scattering solutions for such systems would be problematic for a number of reasons. For example, application of the CI-Kohn approach [5] to determine the phase shifts for positron scattering from any group II or IIB atom would result in linear equations with dimensions between 400,000 to 1,000,000. These are simply too large to be solved by direct methods. Iterative methods for large linear systems do exist, but there are no robust methods that absolutely guarantee convergence [17]. The development of an efficient linear solver for the class of problems that arise from a basis set treatment of quantum scattering would likely involve a good deal of initial experimentation and effort. Similarly, the widely used R -matrix method with fixed boundary conditions [7] requires the generation of all the eigenvectors and eigenvalues of the Hamiltonian, which is not feasible when the matrix dimensions exceed 100,000.

Very recently, a method was developed to extract phase shifts from the positive energies of a pair of CI calculations [18]. In that work, the energy shifts of a positive energy pseudo-state were used to tune a semi-empirical optical potential which was then used to predict the close to threshold phase shifts. This concept is refined in the present work and it is shown that the reliability of the potential can be enhanced by tuning the potential to the energies of the two lowest states. Next, the s - and p -wave phase shifts for positron scattering from Mg and Zn are computed from threshold to the opening of the lowest energy excitation channel. The Mg and Zn atoms are interesting for positron scattering experiments since Mg

*Electronic address: jxm107@rsphysse.anu.edu.au

†Electronic address: mbromley@physics.sdsu.edu

has been recently shown to possess a prominent p -wave shape resonance [18]. The Zn system is also interesting since the existence of a $e^+\text{Zn}$ bound state of $^2\text{S}^e$ symmetry [19] will manifest itself in a differential cross section that is largest at backward angles [20].

I. MODEL INDEPENDENT METHOD FOR GENERATING PHASE SHIFTS

A. The box variational method

The idea behind the current method lies closest to the box variational method [21, 22, 23] which is exploited in quantum Monte Carlo (QMC) calculations of scattering [24, 25, 26, 27, 28]. In the box variational method, one extracts the phase shift by comparing the zero point energy of a finite size cavity to the energy of the system wave function in the same cavity. In its simplest incarnation for s -wave scattering, one diagonalizes the Hamiltonian, in natural units where $\hbar = m = e = 1$,

$$H = -\frac{1}{2}\nabla^2 + V(r), \quad (1)$$

in a cavity of radius R . The wave function obeys the boundary conditions $\Psi(0) = \Psi(R) = 0$. The positive energy states $\Phi_n(r)$, with energy E_n , can be regarded as the small r -part of the exact scattering wave function, $\Psi_n(r)$, with that same energy. The exact wave function can be written as $\Psi_n(r) = \sin(k_n r + \delta)$ for $r > R$ where δ is the phase shift and the wavenumber $k_n = \sqrt{2E_n}$. At the boundary, one has $\sin(k_n R + \delta) = 0$, giving

$$\delta = n\pi - k_n R, \quad (2)$$

(this expression assumes there are no bound states).

For systems with non-zero angular momentum, the asymptotic sin-wave is replaced by the asymptotic form $\psi(r) \sim j_\ell(kr) + \tan(\delta_\ell)n_\ell(kr)$ where $j_\ell(kr)$ and $n_\ell(kr)$ are spherical Bessel functions of the 1st and 2nd kind. The condition $\psi(R) = 0$ gives the following expression for the phase shift,

$$\tan(\delta_\ell(k_n)) = -\frac{j_\ell(k_n R)}{n_\ell(k_n R)}. \quad (3)$$

B. Phase shifts using pseudo-state energy shifts.

The box variational method has two advantages, (a) it is very simple to apply and (b) the B -spline basis sets currently in use in many atomic structure applications easily satisfy the necessary boundary conditions. However, there are other basis sets in use that do not satisfy the $\Psi(0) = \Psi(R) = 0$ boundary conditions.

Consider the usage of a set of general L^2 functions, $u = \{\phi_i\}$. These functions have a finite radial extent and thus the basis can be regarded as defining a soft-sided cavity.

A simple procedure is used here to estimate the radius of the resulting soft-sided box. Denoting $E[u, 0]_n$ to be the n th energy eigenstate resulting from a diagonalization of the $V = 0$ potential in the basis u , then the effective radius of the soft box is given by

$$R = \frac{X_{\ell n}}{\sqrt{2E[u, 0]_n}} = \frac{X_{\ell n}}{k[u, 0]_n}, \quad (4)$$

where $X_{\ell n}$ is the n th zero of the spherical Bessel function, $j_\ell(x)$.

The potential $V = V(r)$ is then diagonalized in the same basis to give $E[u, V]_n$, and hence $k[u, V]_n = \sqrt{2E[u, V]_n}$. The phase shift is then extracted using

$$\tan(\delta_\ell) = -\frac{j_\ell(k[u, V]_n R)}{n_\ell(k[u, V]_n R)}. \quad (5)$$

Figure 1 shows the radial probability density, $|\Psi(r)|^2 = |\sum_\alpha c_\alpha r \chi_\alpha|^2$, of the four lowest energy $\ell = 0$ wave functions computed by the diagonalization of a $V = 0$ potential in a basis of 30 Laguerre Type Orbitals (LTOs) with the scale parameter $\lambda = 1$. The general definition for the LTOs were

$$\chi_\alpha(r) = N_\alpha r^\ell \exp(-\lambda_\alpha r) L_{n_\alpha - \ell - 1}^{(2\ell + 2)}(2\lambda_\alpha r), \quad (6)$$

where the normalization constant is

$$N_\alpha = \sqrt{\frac{(2\lambda_\alpha)(n_\alpha - \ell - 1)!}{(\ell + n_\alpha + 1)!}}. \quad (7)$$

The function $L_{n_\alpha - \ell - 1}^{(2\ell + 2)}(2\lambda_\alpha r)$ is an associated Laguerre polynomial that can be defined in terms of a confluent hyper-geometric function [29]. The probability densities go to zero for $r > 60$. The wiggles in the probability densities are not a numerical artifact, rather they are a manifestation of the slow convergence of the L^2 basis to the exact continuum wave function [30].

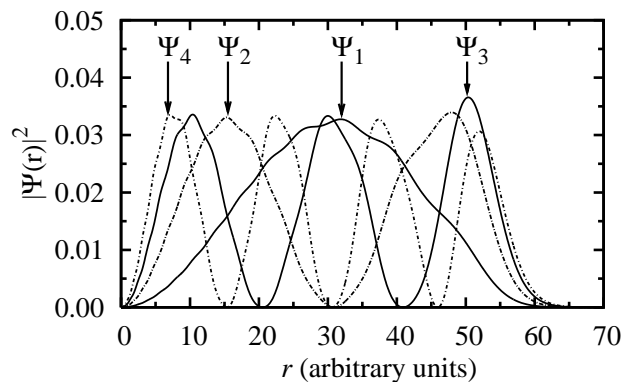


FIG. 1: The radial probability densities, $|\Psi(r)|^2$, for the four lowest s -wave pseudo-states resulting from a diagonalization of the $V = 0$ potential in a basis of 30 LTOs. The pseudo-states have all been normalized to unity.

Table I gives the energies, and the effective radius, of the soft box for this basis as given by eq. (4). The four states have an effective radius of about 61.5 which is consistent with Figure 1. It is reasonable to conclude that eq. (4) gives an estimate of the range of a pseudo-state that is sufficiently accurate to be useful.

This LTO basis was also used to diagonalize the Woods-Saxon potential,

$$V(r) = -\frac{V_0}{1 + \exp\left(\frac{r-W_0}{a}\right)}, \quad (8)$$

with the choice $V_0 = 0.97$, $W_0 = 1$ and $a = 0.05$. The energies and phase shifts derived from eq. (5) are listed in Table I. The phase shifts obtained by numerically integrating the Schrödinger equation for the Woods-Saxon potential are also listed in Table I and are exact to all quoted digits. The two sets of phase shifts agree with each other to an accuracy of about 2%.

TABLE I: Parameters derived from the diagonalization of the free-wave and Woods-Saxon potential in a basis of 30 LTOs with $\lambda = 1$. The pseudo-state energies for $V = 0$ is denoted E_0 while the Woods-Saxon energies are denoted E_{ws} . The radius of the soft-box is denoted R_0 , while the phase shift from eq. (5) is δ . The phase shift obtained by integrating the Woods-Saxon potential numerically is δ_{exact} .

n	E_0	R_0	E_{ws}	δ	δ_{exact}
$\ell = 0$					
1	0.001286	61.95	0.001170	0.1451	0.1470
2	0.005170	61.79	0.004705	0.2897	0.2852
3	0.011734	61.52	0.010736	0.4098	0.4092
4	0.021116	61.15	0.019362	0.5333	0.5148
$\ell = 1$					
1	0.002474	63.87	0.002450	0.0212	0.0211
2	0.007361	63.67	0.007147	0.1114	0.1103
3	0.014810	63.36	0.013964	0.3132	0.3073
4	0.024969	62.94	0.022844	0.6087	0.5903

This procedure has also been validated for p -wave scattering. Figure 2 shows the result of diagonalizing the $V = 0$ potential for p -wave scattering in a basis of 30 LTOs with $\ell = 1$ and $\lambda = 1.0$. Once again the range of the pseudo-state solutions are roughly the same. Table I lists the effective box radius for each pseudo-state as derived from eq. (4).

The Woods-Saxon potential with the choice $V_0 = 0.173$, $W_0 = 4.0$ and $a = 1.0$ was then diagonalized in this basis. The phase shifts obtained from eq. (5) are tabulated in Table I along with phase shifts generated by a numerical solution of the Schrödinger equation. The two sets of phase shifts agree to within 3%.

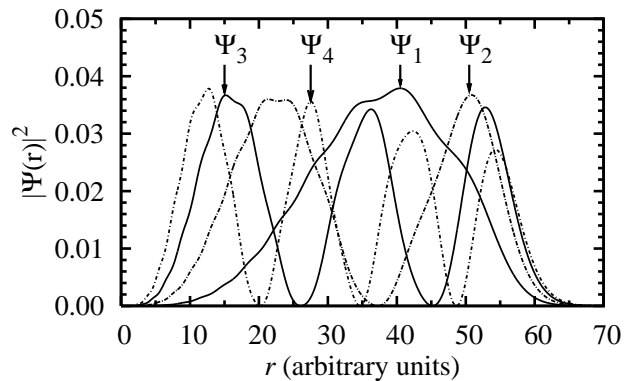


FIG. 2: The radial probability densities, $|\Psi(r)|^2$, for the four lowest p -wave pseudo-states resulting from a diagonalization of the $V = 0$ potential in a basis of 30 LTOs. The pseudo-states have all been normalized to unity.

II. MODEL DEPENDENT METHOD FOR GENERATING PHASE SHIFTS

It has long been known that the positive energy pseudo-states resulting from the diagonalization of the Hamiltonian in an L^2 basis often give a reasonable approximation to the exact scattering wave function over a finite range [31, 32, 33, 34, 35, 36]. Methods which exploit this result are sometimes called stabilization methods. While convergence of the pseudo-state to the continuum wave function is relatively slow, matrix elements formed by the pseudo-state often have reasonable convergence properties [30]. In effect, while the point-wise properties of the wave function can be inaccurate, the convergence in the mean of the wave function over a suitable range can be quite good. This raises the possibility that the expectation values of positive energy pseudo-states can be used to define a semi-empirical optical potential to describe low-energy scattering.

Our method proceeds as follows. The initial calculation uses a reference basis of square integrable single particle orbitals, $\{\phi_i(\mathbf{r})\}$, designed to give a good representation of the wave function in a bounded interaction region. The Hamiltonian, H_0 for a free particle with $V = 0$ is diagonalized, yielding the wave function

$$\Phi_0 = \sum_i c_i \phi_i(\mathbf{r}), \quad (9)$$

and the energy expectation,

$$E_{\text{free}} = \langle \Phi_0 | H_0 | \Phi_0 \rangle. \quad (10)$$

The wave function of the target atom is constructed from a linear combination of configurations $\{\omega_i(\mathbf{X})\}$, of the same symmetry as the ground state (\mathbf{X} is the collective set of target coordinates). So one can write

$$\Omega_{\text{gs}}(\mathbf{X}) = \sum_i c_i \omega_i(\mathbf{X}), \quad (11)$$

while

$$E_{\text{gs}} = \langle \Omega_{\text{gs}} | H_{\text{target}} | \Omega_{\text{gs}} \rangle. \quad (12)$$

The reference energy, E_0 , is determined by diagonalizing the Hamiltonian in the product basis, $\Omega_{\text{gs}}(\mathbf{X})\phi_i(\mathbf{r})$, to give

$$E_0 = \langle \Psi_0 | H_{\text{target}} | \Psi_0 \rangle, \quad (13)$$

where

$$\Psi_0 = \sum_i c_i \phi_i(\mathbf{r}) \Omega_{\text{gs}}(\mathbf{X}). \quad (14)$$

The basis sets $\{\phi_i(\mathbf{r})\}$ and $\{\omega_i(\mathbf{X})\}$ are then augmented by a large number of additional functions $\{\chi_i(\mathbf{r})\}$ and $\{\psi_i(\mathbf{X})\}$ to represent the correlations between the projectile and the target constituents. None of these additional functions have the same symmetries as those used in $\{\phi_i(\mathbf{r})\}$ and $\{\omega_i(\mathbf{X})\}$. This augmented trial function can be written as

$$\Psi_1 = \sum_{i,j} c_{i,j} \omega_i(\mathbf{X}) \phi_j(\mathbf{r}) + \sum_{i,j} d_{i,j} \psi_i(\mathbf{X}) \chi_j(\mathbf{r}). \quad (15)$$

The trial wave function, Ψ_1 , is used to diagonalize H_{exact} giving an energy

$$E_1 = \langle \Psi_1 | H_{\text{exact}} | \Psi_1 \rangle. \quad (16)$$

Next, the basis $\{\phi_i(\mathbf{r})\}$ is diagonalized in a parameterized potential designed to describe the most important features of the interaction between the projectile and the target. This potential can be written formally as

$$V_{\text{opt}}(r) = V_{\text{dir}}(r) + V_{\text{pol}}(r). \quad (17)$$

The potential V_{dir} is the direct interaction between the target and projectile. This can be approximated by the direct interaction between the projectile and the target Hartree-Fock (HF) ground state wave function, Ω_{HF} , which can be slightly different from Ω_{gs} . The polarization potential $V_{\text{pol}}(r)$ is semi-empirical in nature with the asymptotic form

$$V_{\text{pol}}(r) \sim -\frac{\alpha_d}{2r^4}, \quad (18)$$

where α_d is the static dipole polarizability of the target. In previous work, [18, 20, 37, 38] a simple one-parameter form

$$V_{\text{p1}}(r) = -\frac{\alpha_d}{2r^4} (1 - \exp(-r^6/\rho^6)), \quad (19)$$

has usually been adopted for $V_{\text{pol}}(r)$. It is thought that this functional form has the incorrect shape at intermediate values of r , e.g. $r \approx 5 a_0$ (The reasons why we originally become suspicious about the reliability of eq. (19) are not discussed here. But the results obtained later will clearly show the limitations of this type of cutoff polarization potential). The present work will also use a more

complicated expression for $V_{\text{pol}}(r)$, with an additional adjustable parameter, A_Q to give an improved description of the potential between target and atom. This form was

$$V_{\text{p2}}(r) = -\frac{\alpha_d}{2r^4} (1 - \exp(-r^6/\rho^6)) - \frac{A_Q}{2r^6} (1 - \exp(-r^8/\rho^8)). \quad (20)$$

While the second term has the functional form of a quadrupole polarization potential, it should be regarded as primarily empirical in nature. This functional form was chosen as a screened quadrupole type potential because it was computationally convenient.

The energy expectation value of the ground state, or lowest energy pseudo-state

$$E_{\text{opt}} = \langle \Phi_{\text{opt}} | H_{\text{opt}} | \Phi_{\text{opt}} \rangle, \quad (21)$$

is adjusted by tuning the parameters in V_{p1} until $E_{\text{opt}} = E_1 - E_{\text{gs}}$.

Determination of the V_{p2} required additional information since there are two parameters, ρ and A_Q that need to be fixed. In this case, the optical potential is tuned to two energy levels rather than one. This does increase the overall time of the calculation since it is necessary to extract the lowest two eigenvalues from the CI calculation.

Once the optical potential has been fixed, it is a simple matter to generate the exact continuum solution of the Schrödinger equation for the Hamiltonian given by eq. (17).

A. Positron annihilation

Besides obtaining the phase shifts in the low-energy region, it is also possible to determine the annihilation parameter, Z_{eff} [10, 39, 40]. The fundamental idea is to compare exact and model potential calculations of Z_{eff} , and so fix the enhancement factor, G [38, 41, 42]. Enhancement factors were first introduced in the calculation of the annihilation rate of positrons in condensed matter systems [43, 44, 45]. They incorporate the tendency for attractive electron-positron correlations to increase the electron density at the position of the positron.

It has been shown that model potential calculations of s -wave positron scattering from hydrogen and helium that were tuned to give the correct phase-shift at a reference energy also reproduced the low-energy behavior of $Z_{\text{eff}}(k)$ up to a multiplying constant (i.e. G) [38]. The annihilation parameter for the model potential wave function follows the model of Mitroy and Ivanov [38], and is written as

$$Z_{\text{eff}} = \int d^3r (G_v \rho_v(\mathbf{r}) + G_c \rho_c(\mathbf{r})) |\Phi_{\text{opt}}(\mathbf{r})|^2, \quad (22)$$

where $\rho_c(\mathbf{r})$ and $\rho_v(\mathbf{r})$ are the electron densities associated with the core and valence electrons of the target

atom, and $\Phi_{\text{opt}}(\mathbf{r})$ is the positron scattering function obtained in the tuned model potential. The notation $Z_{\text{eff}}^{(\ell)}$ is used to denote the annihilation parameter for the ℓ th partial wave.

For the core orbitals, G_c is set to 2.5 due to reasons outlined in Ref. [38]. The valence enhancement factor G_v is computed by the simple ratio

$$G_v = \frac{\Gamma_v^{CI}}{\Gamma_v^{\text{model}}}, \quad (23)$$

where Γ_v^{CI} is the annihilation rate of the positron with the valence orbitals as given by the CI calculation and Γ_v^{model} is the valence annihilation rate predicted by the model potential calculation with $G = 1$.

III. THE FIXED CORE POTENTIALS

All calculations on the $e^+\text{Cu}$, $e^+\text{Mg}$, and $e^+\text{Zn}$ systems used a fixed core Hamiltonian. The details of the core potentials have been discussed previously [20, 29, 46, 47, 48], but a short description is worthwhile. The model Hamiltonian is initially based on a HF wave function for the neutral atom ground state. One and two-body semi-empirical polarization potentials are added to the potential field of the HF core and the parameters of the core-polarization potentials defined by reference to the spectra of Cu, Mg^+ and Zn^+ [20, 29, 46, 47].

The effective Hamiltonian for the systems with 2 valence electrons (\mathbf{r}_1 and \mathbf{r}_2) and a positron (\mathbf{r}_0) was

$$\begin{aligned} H = & -\frac{1}{2}\nabla_0^2 - \sum_{i=1}^2 \frac{1}{2}\nabla_i^2 - V_{\text{dir}}(\mathbf{r}_0) + V_{\text{cp1}}(\mathbf{r}_0) \\ & + \sum_{i=1}^2 (V_{\text{dir}}(\mathbf{r}_i) + V_{\text{exc}}(\mathbf{r}_i) + V_{\text{cp1}}(\mathbf{r}_i)) - \sum_{i=1}^2 \frac{1}{r_{i0}} \\ & + \frac{1}{r_{12}} - V_{\text{cp2}}(\mathbf{r}_1, \mathbf{r}_2) + \sum_{i=1}^2 V_{\text{cp2}}(\mathbf{r}_i, \mathbf{r}_0). \end{aligned} \quad (24)$$

The direct potential (V_{dir}) represents the interaction with the HF electron core. The direct part of the core potential is attractive for electrons and repulsive for the positron. The exchange potential (V_{exc}) between the valence electrons and the HF core was computed without approximation.

The one-body core polarization potentials (V_{cp1}) are semi-empirical in nature. They have the functional form

$$V_{\text{cp1}}(r) = - \sum_{\ell m} \frac{\alpha_d g_\ell^2(r)}{2r^4} |\ell m\rangle \langle \ell m|. \quad (25)$$

The factor α_d is the static dipole polarizability of the core and $g_\ell^2(r)$ is a cut-off function designed to make the polarization potential finite at the origin. The same cut-off function has been adopted for both the positron and electrons. In this work, $g_\ell^2(r)$ was defined to be

$$g_\ell^2(r) = 1 - \exp(-r^6/\rho_\ell^6), \quad (26)$$

where ρ_ℓ is an adjustable parameter. The two-body polarization potential (V_{cp2}) is defined as

$$V_{\text{cp2}}(\mathbf{r}_i, \mathbf{r}_j) = \frac{\alpha_d}{r_i^3 r_j^3} (\mathbf{r}_i \cdot \mathbf{r}_j) g_{\text{cp2}}(r_i) g_{\text{cp2}}(r_j). \quad (27)$$

where $g_{\text{cp2}}(r)$ is chosen to have a cut-off parameter, ρ_{cp2} , obtained by averaging the ρ_ℓ . The core dipole polarizabilities were set to $0.4814 a_0^3$ for Mg [29, 46], $5.36 a_0^3$ for Cu [47], and $2.294 a_0^3$ for Zn [20]. The cutoff parameters for Mg were $\rho_0 = 1.1795 a_0$, $\rho_1 = 1.302 a_0$, $\rho_2 = 1.442 a_0$, $\rho_3 = 1.52 a_0$, $\rho_{\ell \geq 4} = 1.361 a_0$, and $\rho_{\text{cp2}} = 1.361 a_0$. The cutoff parameters for Cu were $\rho_0 = 1.9883 a_0$, $\rho_1 = 2.03 a_0$, $\rho_2 = 1.83 a_0$, $\rho_3 = 1.80 a_0$, $\rho_{\ell \geq 4} = 1.91 a_0$, and $\rho_{\text{cp2}} = 1.91 a_0$. The cutoff parameters for Zn were $\rho_0 = 1.63 a_0$, $\rho_1 = 1.80 a_0$, $\rho_2 = 2.30 a_0$, $\rho_3 = 1.60 a_0$, $\rho_{\ell \geq 4} = 1.83 a_0$, and $\rho_{\text{cp2}} = 1.83 a_0$. This model has been used to describe many of the features of neutral Be, Mg, Ca and Sr to quite high accuracy [29, 46, 49].

IV. VERIFICATION FOR $e^+\text{-Cu}$ SCATTERING

Previously, a validation of the method was performed for s -wave $e^+\text{-H}$ scattering [18]. In the present work the method is further verified by computing the low-energy phase shifts and annihilation parameters for s -wave and p -wave $e^+\text{-Cu}$ scattering. The model copper atom used here has a dipole polarizability of $41.65 a_0^3$ [29] and, therefore, provides a more stringent test of the procedure used to tune the shape of the polarization potential than the previous test upon the $e^+\text{-H}$ system (where $\alpha_d = 4.5 a_0^3$).

The explicit CI calculation on the $e^+\text{-Cu}$ ground state and the CI-Kohn calculations of $e^+\text{-Cu}$ scattering closely follow those previously reported [5, 47, 48]. Briefly, the wave function expansion consists of a large number of single particle orbitals and includes terms with $\ell > 10$. The single particle orbitals are usually represented as Laguerre type orbitals (LTOs).

The $e^+\text{Cu}$ ground state calculation included orbitals up to $L \leq 16$ with a minimum of 18 electron LTOs and 18 positron LTOs per ℓ . The CI reference wave function, Ψ_0 , consisted of the copper atom ground state multiplied by a positron basis of 30 $\ell = 0$ LTOs. The orbital basis was slightly reduced for the calculation of the lowest energy $^2\text{P}^o$ pseudo-state. In this case, the calculation included terms up to $L = 14$ with a minimum of 18 electron LTOs and 18 positron LTOs per ℓ . The CI reference wave function, Ψ_0 , in this case consisted of the copper atom ground state multiplied by a positron basis of 33 $\ell = 1$ orbitals.

One difficulty present in all CI calculations of positron-atom interactions is the slow convergence of the energy with L [14, 48, 50]. The convergence pattern of the atomic CI expansion [48, 51, 52, 53, 54, 55, 56], suggests the use of an asymptotic analysis that utilizes the result that successive increments, $\Delta E_L = \langle E \rangle_L - \langle E \rangle_{L-1}$, can

TABLE II: Expectations values obtained from CI calculations of the bound ${}^2S^e$ states and the ${}^2P^o$ pseudo-states for the e^+Cu , e^+Mg and e^+Zn systems. The binding energy ε (in Hartree) is negative for bound states and positive for pseudo-states. The mean positron radius $\langle r_p \rangle$ is in units of a_0 . The core ($\langle \Gamma \rangle_c$) and valence ($\langle \Gamma \rangle_v$) annihilation rates are given in units of 10^9 s^{-1} . All of the values given in this table are the results of extrapolating $L \rightarrow \infty$.

System	Symmetry	ε	$\langle r_p \rangle$	$\langle \Gamma \rangle_c$	$\langle \Gamma \rangle_v$
e^+Cu	${}^2S^e$	-0.005124	9.037	0.0322	0.5035
e^+Cu	${}^2P^o$	0.001860	35.23	0.000413	0.0186
e^+Mg	${}^2S^e$	-0.01704	6.930	0.0109	1.004
e^+Mg	${}^2P^o$	0.003989	13.87	0.00110	0.3729
e^+Zn	${}^2S^e$	-0.003794	9.726	0.0244	0.4269
e^+Zn	${}^2P^o$	0.006885	20.24	0.000609	0.0190

be written as an inverse power series, *viz.*

$$\Delta E_L \approx \frac{A_E}{(L + \frac{1}{2})^4} + \frac{B_E}{(L + \frac{1}{2})^5} + \frac{C_E}{(L + \frac{1}{2})^6} + \dots \quad (28)$$

The $L \rightarrow \infty$ limits have been determined by fitting sets of $\langle E \rangle_L$ values to asymptotic series with either 1, 2 or 3 terms. The factors, A_E , B_E and C_E for the 3-term expansion are determined at a particular L from 4 successive energies ($\langle E \rangle_{L-3}$, $\langle E \rangle_{L-2}$, $\langle E \rangle_{L-1}$ and $\langle E \rangle_L$). The series is summed to ∞ once the linear factors have been determined.

Some expectation values of the e^+Cu ${}^2S^e$ ground state and the lowest energy ${}^2P^o$ pseudo-state in the $L \rightarrow \infty$ limits are given in Table II. It should be noted that the leading term of the inverse power series for the annihilation rate, Γ , is $A_\Gamma/(L + 1/2)^2$ [48, 55]. There is some uncertainty in the extrapolation procedure and we estimate uncertainties of about 1% for the energy and 5% for the annihilation rate. However, this does not impact the present verification exercise. The extrapolation procedures were applied consistently to both the CI calculations used to define the model potentials (and enhancement factors), as well as the independent CI-Kohn scattering calculations [5] used to validate the model potential calculations. Note that the errors in the extrapolated results introduced by the use of a finite basis set have a tendency to fortuitously cancel out [48].

The trial function, Ψ_0 , was then used to diagonalize the model potential, eq. (20) with two different polarization potentials. In the first instance, eq. (19) was used and the parameter ρ varied until the energy matched that of the CI calculation. This potential will be referred to as the V_{p1} potential. In the second instance, the parameters, A_Q and ρ of eq. (20) were both varied until both the energy of the ground state and lowest energy pseudo-state were the same as the CI calculations. This potential will be termed the V_{p2} potential. The enhancement factor, G_v , was determined after the model potentials were finalized. In the case of the V_{p2} potential the ratio in

eq. (23) was evaluated for the ground state. The details of the model potential parameters are summarized in Table III.

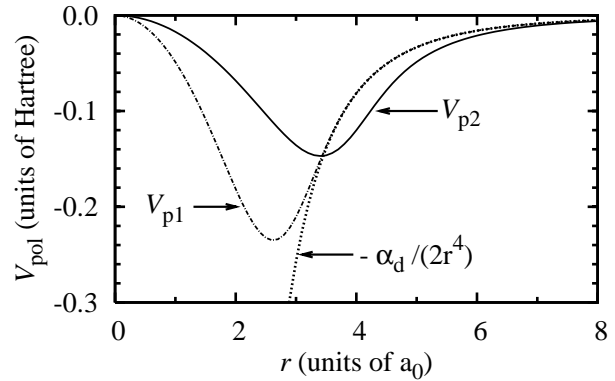


FIG. 3: Comparison of the two different parameterizations of the e^+Cu ${}^2S^e$ polarization potential of eq. (19) and eq. (20) against that of the asymptotic form of eq. (18).

Figure 3 shows a comparison of the V_{p1} and V_{p2} polarization potentials for the ${}^2S^e$ symmetry. The V_{p1} potential is always smaller in magnitude than the $\alpha_d/(2r^4)$ asymptotic form. The V_{p2} potential bulges below the $\alpha_d/(2r^4)$ asymptotic form and is stronger than a pure dipole potential in the outer valence region of the atom. This is entirely reasonable. The slow convergence of the single-center expansion occurs as a result of the localization of the valence electrons in the vicinity of positron [10, 11, 12, 13, 14, 15]. This, in turn, enhances the strength of the polarization potential in the outer valence region.

The superiority of the V_{p2} potential in describing the the ${}^2S^e$ bound state is apparent from Tables II and III. The V_{p2} calculation overestimates the core annihilation rate by 26% while the V_{p1} potential overestimates this parameter by more than 120%. Additionally, the V_{p2} potential gives a better estimate of the mean positron radius, $\langle r_p \rangle$. The value of $8.822 a_0$ is about 2% smaller than the CI value of $9.037 a_0$ while V_{p1} gave $\langle r_p \rangle = 8.46 a_0$ ($\approx 6\%$ smaller).

Accurate phase shifts for the full e^+Cu scattering Hamiltonian were obtained from CI-Kohn variational calculations [5] of the e^+Cu system using *exactly* the same short-range orbital basis sets as used in the CI calculation. The only difference between the CI-Kohn and regular CI basis sets is the addition of two continuum basis functions [5]. The phase shifts for the V_{p1} and V_{p2} potentials were obtained by integrating the Schrödinger equation.

The V_{p2} scattering length estimate of $12.8 a_0$ is within 2% of the CI-Kohn estimate of the scattering length, namely $13.05 a_0$. The V_{p1} scattering length of $12.4 a_0$ is too small by 5%. Figure 4 shows the comparison between the model potential s -wave phase shift and the CI-Kohn phase shift for $k \in [0, 0.2] a_0^{-1}$. The V_{p1} model slightly

TABLE III: Definitions of the V_{p1} and V_{p2} model potentials used to describe s -wave and p -wave scattering of e^+ -Cu, e^+ -Mg and e^+ -Zn. The s -wave potentials were tuned to the properties of the $^2S^e$ ground state and the lowest energy pseudo-state, while the p -wave potentials were tuned to the two lowest energy p -wave pseudo-states. The binding energy ε (in Hartree) is negative for bound states and positive for pseudo-states. The mean positron radius and scattering length, A_{scat} , are in units of a_0 . The core and valence annihilation rates are given in units of 10^9 s^{-1} .

Atom	Potential	L	α_d	A_Q	ρ	G_v	ε	$\langle r_p \rangle$	$\langle \Gamma_c \rangle$	$\langle \Gamma_v \rangle$	A_{scat}
Cu	V_{p1}	0	41.65	0.0	2.7434	18.94	-0.005124	8.46	0.0730	0.5036	12.4
Cu	V_{p2}	0	41.65	480.0	3.6248	26.35	-0.005124	8.822	0.04088	0.5034	12.8
Cu	V_{p1}	1	41.65	0.0	2.1231	20.01	0.0057801	35.18	0.00275	0.0186	
Cu	V_{p2}	1	41.65	360.0	3.0829	36.70	0.0057801	35.22	0.000868	0.0186	
Mg	V_{p1}	0	71.35	0.0	2.9927	13.12	-0.017072	6.21	0.0243	1.004	6.09
Mg	V_{p2}	0	71.35	2280.0	4.4794	24.74	-0.017072	6.982	0.00738	1.004	7.23
Mg	V_{p1}	1	71.35	0.0	2.5626	12.35	0.003989	12.90	0.00654	0.3729	
Mg	V_{p2}	1	71.35	1250.0	3.8406	28.15	0.003989	13.80	0.00115	0.3729	
Zn	V_{p1}	0	41.25	0.0	2.6579	9.91	-0.003794	9.34	0.0412	0.4269	14.3
Zn	V_{p2}	0	41.25	430.0	3.5344	14.35	-0.003794	9.71	0.0219	0.4269	14.7
Zn	V_{p1}	1	41.25	0.0	2.1604	10.45	0.006885	20.21	0.00177	0.0190	
Zn	V_{p2}	1	41.25	252.0	3.0117	17.45	0.006885	20.26	0.000770	0.0190	

overestimates the CI-Kohn phase shifts (modulo π) over the entire range. The V_{p2} fit to the CI-Kohn phase shifts is clearly superior.

Besides obtaining phase shifts, this procedure was used to determine the valence annihilation parameter which is shown in Figures 6 and 7. The V_{p2} enhancement factor of $G_v = 26.35$, gives an s -wave annihilation parameter, $Z_{\text{eff}}^{(0)}$, that is within 5% of the explicit CI-Kohn calculation over the entire energy range. Somewhat surprisingly, the $Z_{\text{eff}}^{(0)}$ from the V_{p1} model is almost the same as that from the V_{p2} model.

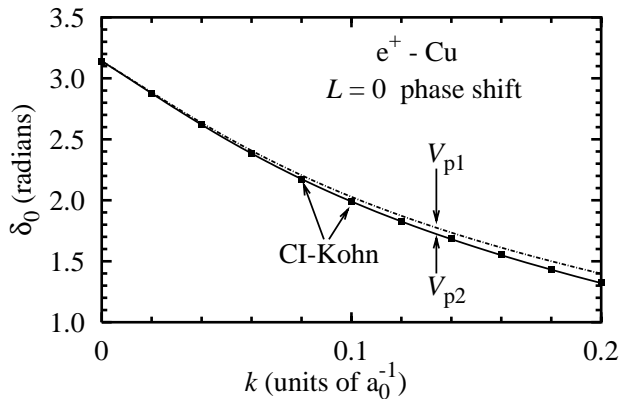


FIG. 4: The phase shift for e^+ -Cu scattering in the s -wave as a function of k (in units of a_0^{-1}). The lines show the results of the present calculation using the tuned V_{p1} and V_{p2} potentials while the squares show the phase shifts of the explicit CI-Kohn calculation.

The phase shift for p -wave scattering is shown in Figure 5. The V_{p1} potential overestimates the CI-Kohn phase shift as the energy increases and there is a 15% discrepancy

at $k = 0.20 a_0^{-1}$. The V_{p1} potential also tends to underestimate the phase shift for $k < 0.10 a_0^{-1}$, although this is difficult to see from the Figure. The V_{p2} potential reproduces the CI-Kohn phase shifts very well and the agreement is perfect within the resolution of the graph.

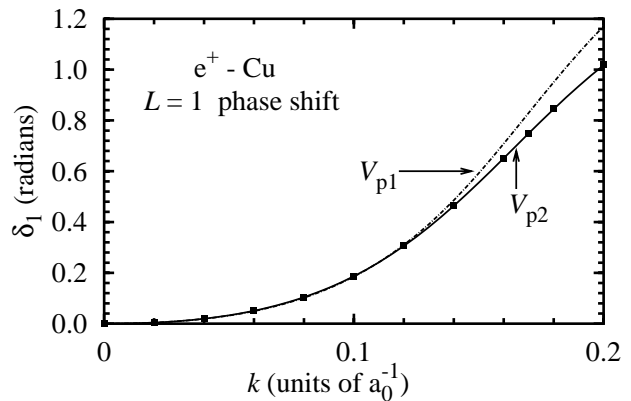


FIG. 5: The phase shift for e^+ -Cu scattering in the p -wave as a function of k (in units of a_0^{-1}). The lines show the results of the present calculation using the tuned V_{p1} and V_{p2} potentials while the squares show the phase shifts of the explicit CI-Kohn calculation.

This pattern is repeated in Figure 7 where $Z_{\text{eff}}^{(1)}$ is plotted as a function of k . The V_{p1} potential tends to overestimate the CI-Kohn values at the higher momenta with the discrepancy at $k = 0.20 a_0^{-1}$ being 15%. However, the V_{p2} potential does an excellent job of reproducing the CI-Kohn $Z_{\text{eff}}^{(1)}$ over the entire momentum range. The V_{p2} $Z_{\text{eff}}^{(1)}$ is too large at the higher momentum, but the difference is only 2% at $k = 0.20 a_0^{-1}$.

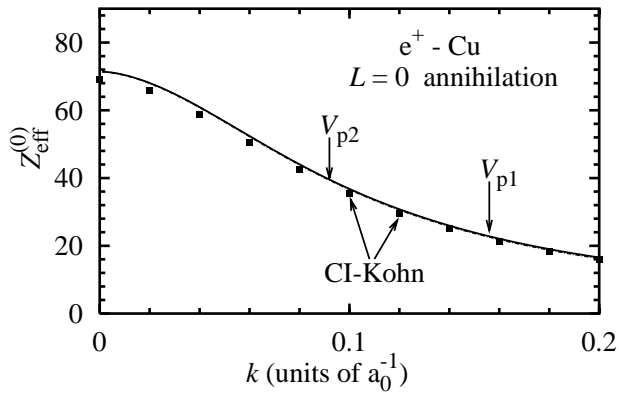


FIG. 6: The annihilation parameter, $Z_{\text{eff}}^{(0)}$ for e^+ -Cu s -wave scattering as a function of k (in units of a_0^{-1}). The two curves were calculated with the V_{p1} and V_{p2} potentials. The discrete points are taken from the explicit CI-Kohn calculations.

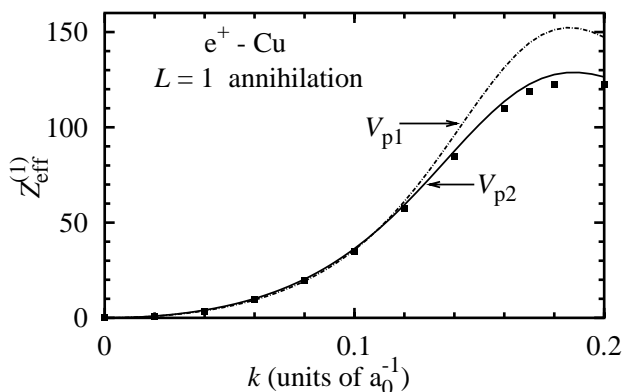


FIG. 7: The annihilation parameter for p -wave scattering, $Z_{\text{eff}}^{(1)}$ for e^+ -Cu scattering as a function of k (in units of a_0^{-1}). The different curves were calculated with the V_{p1} and V_{p2} potentials. The discrete points are taken from the explicit CI-Kohn calculations.

The final confirmation of the improved quality of the V_{p2} potential comes from the comparisons of the pseudo-state expectation values in Tables II and III. The $\langle r_p \rangle$ given by V_{p2} is closer to the CI value than the V_{p1} value. Furthermore, the V_{p2} potential is better than the V_{p1} potential at reproducing the CI core annihilation rate of $0.0322 \times 10^9 \text{ s}^{-1}$ (this value assumes $G_c = 1$).

V. POSITRON SCATTERING FROM MAGNESIUM

A. The CI calculations

Although many of the specifics of the calculations upon e^+ Mg have been reported previously [18, 57], further details concerning the wave function construction are given

here. The trial wave function adopted for the CI calculations consists of a linear combination of states which are anti-symmetric in the interchange of the two electrons,

$$|\Psi; LS\rangle_a = \sum_i c_i |\Phi_i; LS\rangle_a. \quad (29)$$

Each anti-symmetrized state is constructed as a linear combination of coupled but not anti-symmetrized states. Two electrons (particles 1 and 2) are coupled first to each other, then the positron (particle 0) is coupled to form a state with net angular and spin angular momentum, L and S . The anti-symmetric states are written as

$$|\Phi_i; [ab]L_I S_I p L S\rangle_a = \frac{1}{\sqrt{2(1 + \delta_{ab})}} \left(|[a_1 b_2]L_I S_I p_0\rangle + (-1)^{\ell_a + \ell_b + L_I + S_I} |[a_2 b_1]L_I S_I p_0\rangle \right), \quad (30)$$

where the subscript by each orbital denotes the electron occupying that particular orbital.

The e^+ Mg CI basis was constructed by letting the two electrons and the positron form all the possible configuration with a total angular momentum of L , with the two electrons in a spin-singlet state, subject to three selection rules,

$$\max(\ell_0, \ell_1, \ell_2) \leq L, \quad (31)$$

$$\min(\ell_1, \ell_2) \leq L_{\text{int}}, \quad (32)$$

$$(-1)^{(\ell_0 + \ell_1 + \ell_2)} \equiv +1 \text{ or } -1. \quad (33)$$

In these rules ℓ_0 , ℓ_1 and ℓ_2 are respectively the orbital angular momenta of the positron and the two electrons. The even [odd] parity states require $(-1)^{(\ell_0 + \ell_1 + \ell_2)} \equiv +1$ [-1].

The Hamiltonian for the e^+ Mg $2S^e$ state was diagonalized in a CI basis including orbitals up to $\ell = 12$. There were a minimum of 15 radial basis functions for each ℓ . There were 19 $\ell = 0$ positron orbitals. The largest $2S^e$ calculation was performed with $L = 12$ and $L_{\text{int}} = 4$. The L_{int} parameter does not have to be large since it is mainly concerned with describing the more quickly converging electron-electron correlations [46]. The CI basis for the e^+ Mg $2P^o$ symmetry included orbitals up to $\ell = 14$. There were a minimum of 14 radial basis functions for each ℓ . There were 20 $\ell = 1$ positron orbitals. The largest $2P^o$ calculation was performed with $L = 14$ and $L_{\text{int}} = 3$.

A summary of e^+ Mg expectation values taken to the $L \rightarrow \infty$ limit are given in Table II. The binding energy ϵ for each symmetry is calculated with respect to the energy of the Mg ground state using the basis for that symmetry. The overall binding energy of the $2S^e$ ground state was -0.017072 Hartree, with the first pseudo-state at 0.002503 Hartree. The energies of the two lowest pseudo-states of $2P^o$ symmetry were 0.003989 and 0.012012 Hartree respectively.

B. Model potential calculations

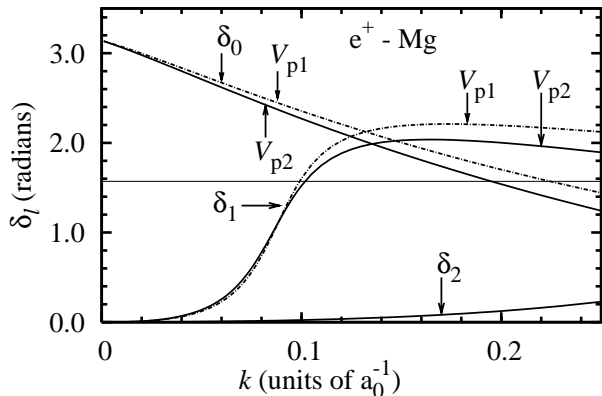


FIG. 8: The s , p and d -wave phase shifts for e^+ -Mg scattering as a function of k (in units of a_0^{-1}). The solid lines were computed with V_{p2} while the dashed lines were computed with V_{p1} . The horizontal line shows $\delta = \pi/2$.

The ρ parameter of the V_{p1} potential was tuned to reproduce the energies of the lowest $^2S^e$ and $^2P^o$ states. The values of ρ and the expectation values of the lowest state of each symmetry are given in Table III. The values of A_Q and ρ for the V_{p2} potential were tuned to the lowest two energies. Examination of the expectation values of Tables II and III reveals that the V_{p2} potential again does a better job at reproducing the CI expectation values. The V_{p1} potential underestimates the mean positron radius by 10% and further overestimates the core annihilation rate by a factor of 2. The V_{p2} potential gives a value of $\langle r_p \rangle$ that is too large by 1%. The V_{p2} underestimation of Γ_c is about 30%. While the V_{p2} model potential may not be perfect, it does a better job of describing the radial distribution of the positron density than the V_{p1} potential.

The situation for the $^2P^o$ pseudo-state is similar to that for the $^2S^e$ state. The V_{p1} potential underestimates the mean positron radius by 10% and overestimates the core annihilation rate by a factor of 6. The V_{p2} potential on the other hand gives an $\langle r_p \rangle$ within 1% of the CI value and overestimates the core annihilation rate by only 5%.

The s - and p -wave phase shifts are plotted in Figure 8. The 10% difference between the two model potential scattering lengths manifests itself in the slightly different s -wave phase shifts. The difference between the V_{p1} and V_{p2} potentials is larger for the p -wave phase shift, although both predict a resonance at $k \approx 0.09 a_0^{-1}$. The d -wave phase shift plotted in Figure 8 was computed with the V_{p2} p -wave potential. The $\ell > 2$ phase shifts used in the computation of the total cross section also used the V_{p2} p -wave potential.

Figure 9 shows the elastic cross section for e^+ -Mg scattering below the Ps formation threshold (at $k \approx 0.25 a_0^{-1}$) as computed with the V_{p2} potentials. The p -wave reso-

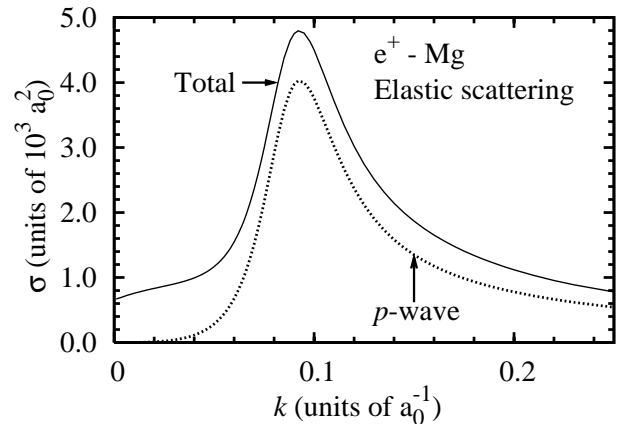


FIG. 9: The elastic scattering cross section for e^+ -Mg scattering as calculated with the V_{p2} potential in the energy region below the Ps-formation threshold at $k \approx 0.249 a_0^{-1}$. The solid line shows the total cross section while the dashed curve shows the $\ell = 1$ partial cross section.

nance leads to the total elastic cross section achieving a peak value of $4800 a_0^2$.

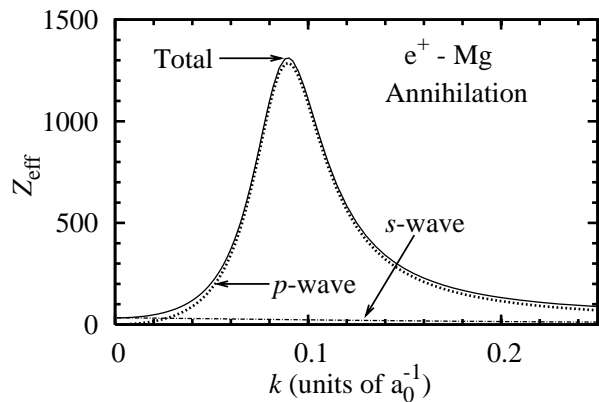


FIG. 10: The annihilation parameter Z_{eff} for e^+ -Mg scattering as a function of k (in units of a_0^{-1}). The different curves show, $Z_{\text{eff}}^{(0)}$, $Z_{\text{eff}}^{(1)}$ and $Z_{\text{eff}}^{(\text{total})}$ as calculated with the V_{p2} potential.

The existence of the resonance in the phase shift also leads to a resonance in the annihilation parameter, Z_{eff} [18]. The curve in Figure 10 was computed with an enhancement factor of $G_c = 2.5$ for core annihilation, an s -wave valence enhancement factor of $G_v = 24.7$ and a p -wave enhancement factor of $G_v = 28.2$. The total Z_{eff} shown in Figure 10 is almost completely dominated by the contribution from the p -wave and the value of Z_{eff} at the resonance peak was 1310.

The resonance parameters were determined by performing a fit to the function

$$\delta = \delta_0 + a(E - \varepsilon_R) + \tan^{-1} \left(\frac{\Gamma}{2(\varepsilon_R - E)} \right) + bE^2. \quad (34)$$

This gave a value of $\varepsilon_R = 0.00351$ Hartree for the resonance position and a width of $\Gamma = 0.00390$ Hartree.

C. Reliability of the resonance prediction

The possible sources of error in the e^+ -Mg calculations are (a) the reliability of the underlying model potential for the CI calculation, (b) the extent to which the CI calculations have converged and (c) the ability of the scattering model potential to reliably reproduce the scattering parameters.

The cutoff parameter for the positron part of the core polarization potential (refer to eq. (25)) is chosen to be the same as the cutoff for the electron. This is likely to underestimate the strength of the positron interaction since there is a good deal of evidence for closed shell systems that suggests the positronic part of the polarization potential is stronger than the electronic part [50]. However, the impact of this is likely to be small since the core polarizability of $0.4814 a_0^3$ is more than 100 times smaller than the neutral atom polarizability of $71.35 a_0^3$. Any correction would tend to shift the resonance to a lower energy and increase the height of the maximum in the cross section.

The CI calculations of the ${}^2S^e$ ground state are believed to be converged to about 2% in the energy. An independent calculation of the e^+ Mg ground state has been done with the fixed core stochastic variational method (FCSVM) [58]. The FCSVM Hamiltonian is very similar to the fixed core Hamiltonian used for the present calculation and the current best FCSVM estimate of the binding energy is 0.017117 Hartree. However, it has also proved possible to make an estimate of the variational limit of the FCSVM calculation. This estimate is between 0.01735 and 0.01740 Hartree [58] which is about 2% more tightly bound than the CI calculation. The calculation of the ${}^2P^o$ state is expected to have an accuracy similar to that of the ground state.

The existence and position of the resonance is independent of the exact form of V_{pol} . Besides the calculations reported here, alternate calculations with some other parameterizations were reported earlier [18]. All of these calculations gave a resonance almost at the same position and magnitude. The reason for this lies in the accident that the energy of the ${}^2P^o$ pseudo-state, at $k = 0.0893 a_0^{-1}$, lies close to the center of the resonance. At this energy, the determination of the phase shift will be largely model independent since the stabilization concept ensures that the L^2 wave function is a reasonable approximation to the actual continuum wave function. The phase shifts of the two potentials at the energy of the pseudo-state were $\delta_1 = 1.157$ and $\delta_1 = 1.153$ radians, for V_{p1} and V_{p2} respectively. Additional plots of the phase shifts obtained with other functional forms for V_{pol} have tended to have a common intersection point near $k \approx 0.089 a_0^{-1}$.

Finally, the simple potential independent approach of

eq. (5) has been applied to determine the phase shift at the pseudo-state energy. The energy of the positron p -wave LTO basis in the $V = 0$ potential was 0.007572 Hartree. The radius of the box giving this energy is $R_{\text{box}} = 36.5 a_0$. Evaluating eq. (5) at $k = 0.0893 a_0^{-1}$ gives $\delta = 1.16$ radian.

VI. POSITRON SCATTERING FROM ZINC

Positron binding to zinc has been known with some degree of certainty since 1999 [19, 20] following some earlier, less conclusive, work [59, 60, 61]. The neutral zinc atom has an ionization potential of 0.34523 Hartree [62] and a polarizability of $38.8 \pm 0.8 a_0^3$ [63]. The present model potential for the Zn^{2+} core predicts an ionization potential of 0.33519 Hartree and a polarizability of $41.25 a_0^3$ [20].

The present CI calculations upon the $e^+\text{Zn}$ ground state used the same core potential as the earlier CI calculations [20], but the size of the basis has been enlarged. The maximum number of partial waves has been increased to $L = 12$, the number of LTOs per ℓ has been increased to 16, and finally L_{int} was increased from 3 to 4. The overall dimension of the CI calculation has increased by an order of magnitude. The summary of $e^+\text{Zn}$ expectation values for the series of calculations with increasing L are given in Table IV. The energy of the Zn ground state with respect to the Zn^{2+} core for the electron basis was -0.99549251 Hartree.

An examination of Table IV reveals that the present extrapolated binding energy of 0.0037944 Hartree is within 2% of the previously obtained binding energy. To a certain extent, this high level of agreement is fortuitous. The method used to extrapolate the energy increment to the $L \rightarrow \infty$ limit in Ref. [20] had an inherent tendency to overestimate the binding energy. However, this compensated for the tendency of a finite dimension LTO basis to increasingly underestimate the energy increment as $L \rightarrow \infty$ [48]. The lowest positive energy ${}^2S^e$ pseudo-state had an energy of 0.0024706 Hartree above the Zn ground state.

The Hamiltonian for the $e^+\text{Zn } {}^2P^o$ state was diagonalized in a CI basis including orbitals up to $\ell = 10$. The two electrons were in a spin-singlet state, with a minimum of 16 radial basis functions for each ℓ . There were 20 $\ell = 1$ positron orbitals. The largest calculation was performed with $L = 10$ and $L_{\text{int}} = 3$. The energy of the lowest energy ${}^2P^o$ pseudo-state was 0.006885 Hartree above threshold. Other expectation values for this state are listed in Table II. The second lowest ${}^2P^o$ pseudo-state was located at 0.019055 Hartree.

The parameters for the V_{p1} and V_{p2} potentials, tuned to the CI data in Table II, are listed in Table III. A casual glance at the entries in these two Tables reveals that the V_{p2} potential again does better at reproducing the properties of the ${}^2S^e$ physical state and the ${}^2P^o$ pseudo-state.

The s - and p -wave phase shifts are plotted in Figure

TABLE IV: Results of the CI calculations for e^+ Zn atoms for a given L . The E column gives the energy with respect to the doubly ionized frozen core and ε is the binding energy with respect to the lowest energy dissociation channel at $E = -0.99549251$ Hartree. The radial expectation values (in a_0) of the electron and positron are listed in the $\langle r_e \rangle$ and $\langle r_p \rangle$ columns. The $\langle \Gamma_v \rangle$ and $\langle \Gamma_c \rangle$ columns give the valence and core annihilation rates (in 10^9 sec^{-1}). The results in the row labeled 10^* are taken from an earlier calculation [20]. The results under the heading $L \rightarrow \infty$ incorporate an $L \rightarrow \infty$ correction.

L	N_e	N_p	N_{CI}	$\langle E \rangle_L$	$\langle \varepsilon \rangle_L$	$\langle r_e \rangle_L$	$\langle r_p \rangle_L$	$\langle \Gamma_c \rangle_L$	$\langle \Gamma_v \rangle_L$
0	19	16	3040	-0.97217702	-0.02331549	2.76525	29.69360	0.0002583	0.0002144
1	37	32	11248	-0.99240348	-0.00308903	2.75421	26.43204	0.0009532	0.0023477
2	55	48	30112	-0.99441912	-0.00107339	2.75879	21.51407	0.0037086	0.0144975
3	71	64	58336	-0.99562488	0.00013237	2.77148	16.80037	0.0086564	0.0456435
4	87	80	101264	-0.99653983	0.00104732	2.78651	13.89104	0.0133632	0.0872535
5	103	96	153744	-0.99719181	0.00169930	2.79963	12.32951	0.0167251	0.1279350
6	119	112	210576	-0.99768537	0.00219287	2.80986	11.46661	0.0189393	0.1632760
7	135	128	271248	-0.99805166	0.00255915	2.81770	10.94916	0.0204117	0.1929861
8	151	144	334096	-0.99832262	0.00283011	2.82371	10.61913	0.0214113	0.2176885
9	167	160	398864	-0.99852427	0.00303176	2.82833	10.39734	0.0221079	0.2382207
10	183	176	463632	-0.99867583	0.00318336	2.83190	10.24428	0.0226023	0.2553248
11	199	192	528400	-0.99879107	0.00329856	2.83471	10.13275	0.0229647	0.2696997
12	215	208	593168	-0.99887979	0.00338728	2.83692	10.05093	0.0232336	0.2818534
10^* [20]	104	97	63712	-0.9983995	0.0030385	2.82927	10.32455	0.022292	0.24023
$L \rightarrow \infty$ extrapolations									
Present				-0.9992869	0.0037944	2.8475	9.72595	0.02434	0.42692
Previous [20]				-0.999092	0.003731	2.8451	9.9139	0.02393	0.3927

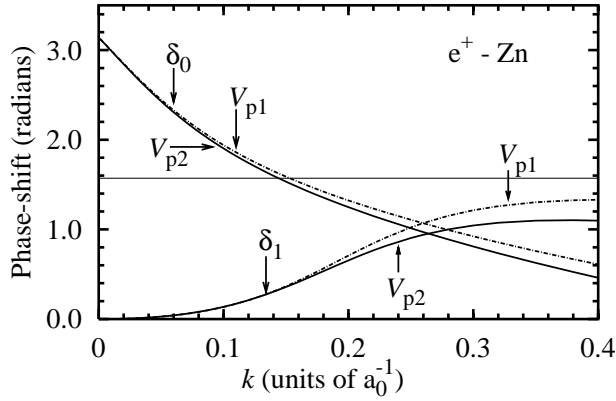


FIG. 11: The s - and p -wave phase shifts for e^+ -Zn scattering as a function of k (in units of a_0^{-1}). The solid lines were computed with V_{p2} while the dashed lines were computed with V_{p1} . The horizontal dashed line shows $\delta = \pi/2$.

11. The small e^+ Zn binding energy leads to a large value for the scattering length, namely $14.7 \pm 0.1 a_0$. The energy region below $k \leq 0.144a_0^{-1}$ would be interesting for an experimental investigation as the s -wave phase shifts are in a different quadrant from all the other phase shifts. Consequently, the differential cross section will be larger at backward angles than at forward angles. This peaking of the near threshold differential cross section at backward angles is a signature of the existence of the e^+ Zn

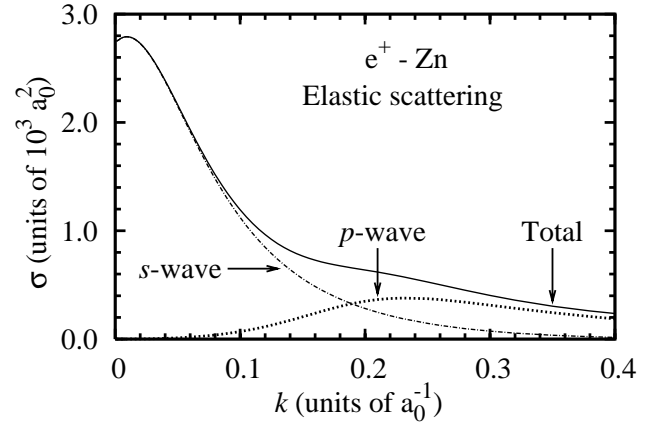


FIG. 12: The elastic scattering cross section for e^+ -Zn scattering as calculated with the V_{p2} potential in the energy region below the Ps-formation threshold at $k \approx 0.436 a_0^{-1}$. The solid line shows the total cross section while the two dashed curves show the $\ell = 0$ and $\ell = 1$ partial cross sections.

bound state [20].

The low-energy elastic cross section below the Ps-formation threshold as shown in Figure 12 was computed with the V_{p2} potentials. The phase shifts for $\ell \geq 1$ are taken from the $\ell = 1$ model potential. The large value of the cross section at $E = 0$ is characteristic of a potential supporting a weak bound state. The quickly rising p -

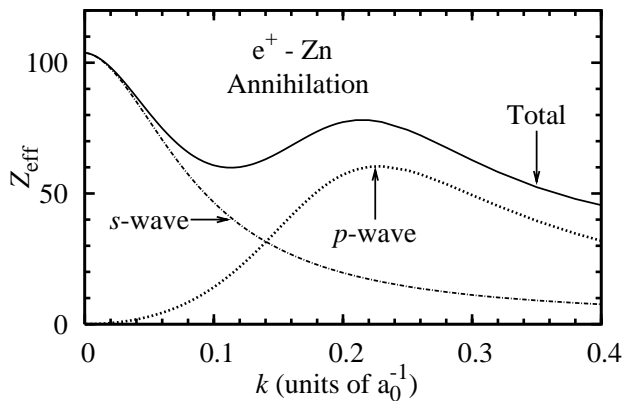


FIG. 13: The annihilation parameter Z_{eff} for e^+ -Zn scattering as a function of k (in units of a_0^{-1}). The different curves show, $Z_{\text{eff}}^{(0)}$, $Z_{\text{eff}}^{(1)}$ and $Z_{\text{eff}}^{(\text{total})}$ as calculated with the V_{p2} potential

wave phase shifts leads to a shoulder in the cross section near $k \approx 0.2 a_0^{-1}$. The p -wave causes a more pronounced structure in Z_{eff} which is easily noticeable in figure 13 as the bump at $k \approx 0.2 a_0^{-1}$.

The experimental observation of the e^+ Zn p -wave resonance precursor in the cross section would be complicated by the large s -wave cross section which tends to obscure the feature in the total elastic cross section. The resonance structure would be most visible in a measurement of Z_{eff} or in a differential cross section.

VII. COMPARISONS WITH PREVIOUS WORK

The present calculations are not the only calculations of the e^+ Mg and e^+ Zn scattering systems. However, the other calculations were of a much more speculative nature [37, 38, 61, 64, 65, 66, 67, 68]. For example, the many body perturbation theory-based calculation of Gribakin and King predicted that the $^2P^o$ symmetry of e^+ Mg had a bound state [66]. None of the other calculations on the e^+ -Mg system gave a cross section with the prominent $^2P^o$ shape resonance.

While some previous model potential calculations were based on reasonable estimates of the e^+ Mg binding energy [37, 38], the uncertainties in defining the functional form of the polarization potential detracted from the reliability of the p -wave phase shift. The present calculations are more definitive, and the main source of uncertainty is in the definition of the underlying core polarization potential in the CI calculations.

VIII. SUMMARY

A new technique has been used to determine the phase shifts for low-energy positron-atom scattering from mag-

nesium and zinc. The phase shifts are determined by tuning an optical potential to the energy of a bound state or a positive energy state. The tuning of an optical potential to features such as bound state energies and resonance positions is well known. Tuning an optical potential to a pseudo-state energy shift is novel [18]. One improvement over our previous implementation is the use of a second energy to fine-tune the shape of the optical potential. Another possible improvement requiring further research would be to use other expectation values (e.g. the mean positron radius) to further refine the shape of the optical potential. The use of experimental information to tune optical potentials is known (e.g. the role of the deuteron radius in tuning the n - p potential).

There are two different concepts that can be regarded as providing motivation for the present approach. The first is the stabilization concept, namely, a positive energy pseudo-state will provide a reasonable approximation to the scattering state with that energy over a finite radial range [31, 32]. The alternate motivation comes from the box variational method, namely that the energy shift of the wave function in a hard-sided box is used to estimate the phase shift [21, 22, 23]. Diagonalization of the Hamiltonian in a finite dimension LTO basis can be regarded as equivalent to diagonalizing the Hamiltonian in a soft-sided box.

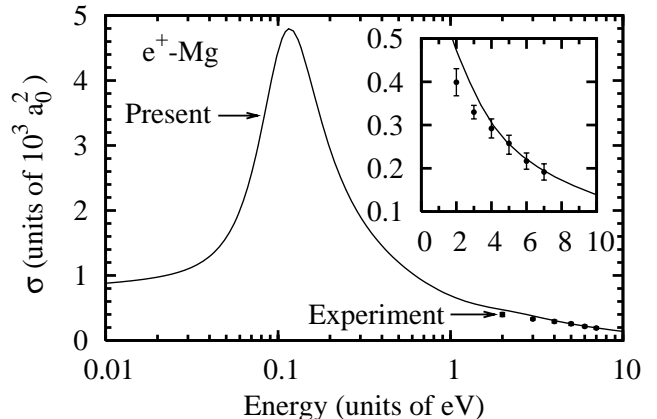


FIG. 14: The cross sections (in $10^3 a_0^2$) for e^+ -Mg scattering versus energy (in eV). The present elastic scattering cross sections as calculated with the V_{p2} potential are shown as the solid line. The total cross section measurements from the Detroit group are shown as the discrete points with their error bars [69]. The inset shows the same data, plotted on a linear energy scale.

The most significant result of the present investigation is the prediction of a close to threshold $^2P^o$ shape resonance for elastic scattering from magnesium. There is no experimental evidence for the existence of shape resonances in positron-atom or positron-molecule scattering [50]. The present prediction has the virtue of being readily amenable to experimental verification. Indeed, the

Detroit group has measured the total cross section for positron-magnesium scattering down to an energy of 2.0 eV [69]. As can be seen from Figure 14, the lowest energy for which their measurements were done is just too high to detect the resonance. An earlier experiment measured down to an energy of 1.0 eV [70], but these results are not shown in the figure as they are similar to those in Ref. [69] whilst having larger reported errors. Their most recent e^+ -Mg measurements went down to 0.12 eV, however, they only reported the positronium formation cross section [71].

With some reflection on the differences between positron-atom and electron-atom interaction potentials it is not surprising that the magnesium atom supports a shape resonance. It has been noticed that the positrons are more strongly attracted to closed (sub)shell atoms than are electrons [50] (this result is based on results for systems with $^2S^e$ symmetry). Since there is a low-energy $^2P^o$ shape resonance in e^- -Mg scattering [72, 73], one could reasonably infer that the e^+ -Mg system would also have a $^2P^o$ shape resonance or, alternatively, support a bound state.

The e^+ -Zn cross section has a broad feature in the p -wave at about 0.6 eV that could be interpreted as a resonance or a precursor to a resonance. It should be noted that a similar feature occurs in e^- -Zn scattering [74] at roughly the same energy. Figure 15 compares the p -wave phase shift from the B-spline R -matrix (BSRM) calculation of e^- -Zn scattering [74] with the present e^+ -Zn phase shift. While the BSRM is probably not converged with respect to the enlargement of the channel space, the low-energy elastic cross section does a reasonable job at reproducing the electron transmission experiment of Burrow *et al* [75]. The similarity between the electron and positron p -wave phase shifts for $k < 0.10 a_0^{-1}$ is expected since the low-energy phase shifts will be dominated by the long range polarization potentials. It is interesting to speculate upon whether the polarization potential will lead to e^+ -Zn phase shifts that are larger than the e^- -Zn phase shifts for the $^2P^o$ symmetry, as well as the $^2S^e$ symmetry. The comparison depicted in Figure 15 shows that the e^- -Zn $^2P^o$ phase shift is larger than the e^+ -Zn phase shift for $k > 0.14 a_0^{-1}$. This is possibly due to the electron seeing an attractive static potential as it penetrates the centrifugal barrier while the positron experiences a repulsive potential. However, it would be best to test this conjecture using models for the Zn target which are exactly the same.

The existence of the e^+ -Mg resonance and the structure in e^+ -Zn suggest that other group II atoms might support a $^2P^o$ shape resonance. The dipole polarizability of beryllium is only a bit smaller than that of Zn, so some sort of structure in the $^2P^o$ partial wave is expected. The cadmium atom, on the other hand has a larger polariz-

ability than zinc, so a more pronounced resonance should be expected.

The actual polarization potentials used here represent a departure from those used in some previous calculations

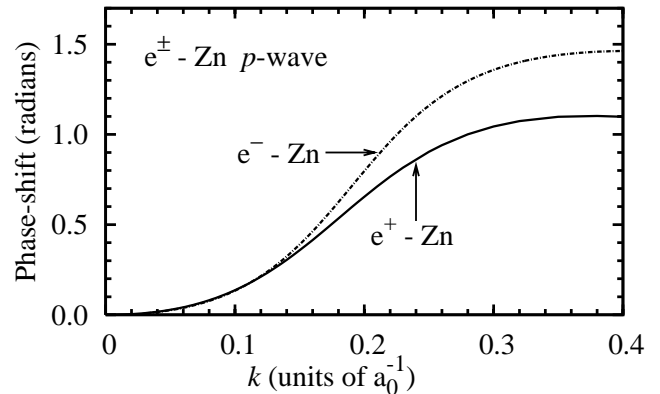


FIG. 15: The p -wave phase shifts as a function of k (in units of a_0^{-1}) for e^\pm -Zn scattering as given by the present calculation and the BSRM calculation [74].

of positron-atom interactions [20, 37, 38, 76, 77]. All of these previous works use polarization potentials with a cut-off function that leads to a potential that is always smaller in magnitude than that of the $\alpha_d/(2r^4)$ asymptotic potential. The present polarization potentials have bulges in the outer valence region that are larger in magnitude than the asymptotic potential in that region.

A possible area of application of the current approach would be to positron-molecule scattering. However, this would require improvements in the technology of positron-molecule CI calculations. The best calculations so far carried out [78, 79, 80] do not treat the electron-positron dynamics nearly as well as the present CI calculations on atoms.

Acknowledgments

This work was supported under the Australian Research Council's Discovery Program (project number 0665020). The authors would like to thank Oleg Zatsarinny and Klaus Bartschat for providing e^- -Zn phase shifts in tabular form. The calculations upon the e^+ Mg and e^+ Zn systems were performed on GNU/Linux clusters hosted at the SDSU Computational Science Research Center and the South Australian Partnership for Advanced Computing (SAPAC). The authors would like to thank Dr. James Otto and Grant Ward for their system administration.

[1] P. G. Burke and C. J. Joachain, *Theory of electron-atom collisions. Part 1 potential scattering* (Plenum, New

York, 1995).

- [2] C. Schwartz, *Ann. Phys. NY* **16**, 36 (1961).
- [3] R. K. Nesbet, *Variational methods in electron-atom scattering theory* (Plenum, New York, 1980).
- [4] B. I. Schneider and T. N. Rescigno, *Phys. Rev. A* **37**, 3749 (1988).
- [5] M. W. J. Bromley and J. Mitroy, *Phys. Rev. A* **67**, 062709 (2003).
- [6] U. Fano and C. M. Lee, *Phys. Rev. Lett.* **31**, 1573 (1973).
- [7] P. G. Burke, A. Hibbert, and W. D. Robb, *J. Phys. B* **5**, 153 (1971).
- [8] R. F. Barrett, B. A. Robson, and W. Tobocman, *Rev. Mod. Phys.* **55**, 155 (1983).
- [9] M. W. J. Bromley and J. Mitroy, *Phys. Rev. Lett.* **97**, 183402 (2006).
- [10] R. P. McEachran, D. L. Morgan, A. G. Ryman, and A. D. Stauffer, *J. Phys. B* **10**, 663 (1977).
- [11] K. Higgins, P. G. Burke, and H. R. J. Walters, *J. Phys. B* **23**, 1345 (1990).
- [12] K. Strasburger and H. Chojnacki, *Chem. Phys. Lett.* **241**, 485 (1995).
- [13] D. M. Schrader, *Nucl. Instrum. Methods Phys. Res. B* **143**, 209 (1998).
- [14] J. Mitroy and G. G. Ryzhikh, *J. Phys. B* **32**, 2831 (1999).
- [15] V. A. Dzuba, V. V. Flambaum, G. F. Gribakin, and C. Harabati, *Phys. Rev. A* **60**, 3641 (1999).
- [16] A. Stathopoulos and C. Froese Fischer, *Comput. Phys. Commun.* **79**, 268 (1994).
- [17] Y. Saad, ed., *Iterative Methods for Sparse Linear Systems* (PWS Publishing, Boston, 2000).
- [18] J. Mitroy and M. W. J. Bromley, *Phys. Rev. Lett.* **98**, 173001 (2007).
- [19] J. Mitroy and G. G. Ryzhikh, *J. Phys. B* **32**, 1375 (1999).
- [20] M. W. J. Bromley and J. Mitroy, *Phys. Rev. A* **65**, 062506 (2002).
- [21] V. Risberg, *Arch. Math. Naturvidenskab* **53**, 1 (1956).
- [22] I. C. Percival, *Proc. Phys. Soc. A* **70**, 494 (1957).
- [23] I. C. Percival, *Phys. Rev.* **119**, 159 (1960).
- [24] Y. Alhassid and S. E. Koonin, *Ann. Phys.* **155**, 108 (1984).
- [25] J. Carlson, V. R. Pandharipande, and R. B. Wiringa, *Nucl. Phys. A* **424**, 47 (1984).
- [26] J. Shumway and D. M. Ceperley, *Phys. Rev. B* **63**, 165209 (2001).
- [27] S. Chiesa, M. Mella, and G. Morosi, *Phys. Rev. A* **66**, 042502 (2002).
- [28] K. M. Nollett, S. C. Pieper, R. B. Wiringa, J. Carlson, and G. M. Hale, *Phys. Rev. Lett.* **99**, 022502 (2007).
- [29] M. W. J. Bromley and J. Mitroy, *Phys. Rev. A* **65**, 012505 (2002).
- [30] A. T. Stelbovics and T. Winata, *Aust. J. Phys.* **43**, 485 (1990).
- [31] F. E. Harris, *Phys. Rev. Lett.* **19**, 173 (1967).
- [32] A. U. Hazi and H. S. Taylor, *Phys. Rev. A* **1**, 1109 (1970).
- [33] R. J. Drachman and S. K. Houston, *Phys. Rev. A* **12**, 885 (1975).
- [34] R. J. Drachman and S. K. Houston, *Phys. Rev. A* **14**, 894 (1975).
- [35] I. A. Ivanov, J. Mitroy, and K. Varga, *Phys. Rev. Lett.* **87**, 063201 (2001).
- [36] I. A. Ivanov, J. Mitroy, and K. Varga, *Phys. Rev. A* **65**, 032703 (2002).
- [37] M. W. J. Bromley, J. Mitroy, and G. Ryzhikh, *J. Phys. B* **31**, 4449 (1998).
- [38] J. Mitroy and I. A. Ivanov, *Phys. Rev. A* **65**, 042705 (2002).
- [39] P. A. Fraser, *Adv. At. Mol. Phys.* **4**, 63 (1968).
- [40] G. G. Ryzhikh and J. Mitroy, *J. Phys. B* **33**, 2229 (2000).
- [41] J. Mitroy and B. Barbiellini, *Phys. Rev. B* **65**, 235103 (2002).
- [42] J. Mitroy, *Phys. Rev. A* **72**, 062707 (2005).
- [43] E. Boronski and R. M. Nieminen, *Phys. Rev. B* **34**, 3820 (1986).
- [44] M. J. Puska and R. M. Nieminen, *Rev. Mod. Phys.* **66**, 841 (1994).
- [45] B. Barbiellini, in *New Directions in Antimatter Physics and Chemistry*, edited by C. M. Surko and F. A. Gianturco (Kluwer Academic Publishers, The Netherlands, 2001), p. 127.
- [46] M. W. J. Bromley and J. Mitroy, *Phys. Rev. A* **65**, 062505 (2002).
- [47] M. W. J. Bromley and J. Mitroy, *Phys. Rev. A* **66**, 062504 (2002).
- [48] J. Mitroy and M. W. J. Bromley, *Phys. Rev. A* **73**, 052712 (2006).
- [49] J. Mitroy and M. W. J. Bromley, *Phys. Rev. A* **68**, 052714 (2003).
- [50] J. Mitroy, M. W. J. Bromley, and G. G. Ryzhikh, *J. Phys. B* **35**, R81 (2002).
- [51] C. Schwartz, *Phys. Rev.* **126**, 1015 (1962).
- [52] D. P. Carroll, H. J. Silverstone, and R. P. Metzger, *J. Chem. Phys.* **71**, 4142 (1979).
- [53] R. N. Hill, *J. Chem. Phys.* **83**, 1173 (1985).
- [54] S. Salomonson and P. Oster, *Phys. Rev. A* **40**, 5559 (1989).
- [55] G. F. Gribakin and J. Ludlow, *J. Phys. B* **35**, 339 (2002).
- [56] M. W. J. Bromley and J. Mitroy, *Int. J. Quantum Chem.* **107**, 1150 (2007).
- [57] M. W. J. Bromley and J. Mitroy, *Phys. Rev. A* **73**, 032507 (2006).
- [58] J. Mitroy and J. Y. Zhang, unpublished (2008).
- [59] R. Szmtykowski, *Acta Phys. Pol. A* **84**, 1035 (1993).
- [60] V. A. Dzuba, V. V. Flambaum, G. F. Gribakin, and W. A. King, *Phys. Rev. A* **52**, 4541 (1995).
- [61] R. P. McEachran and A. D. Stauffer, *Nucl. Instrum. Methods Phys. Res. B* **143**, 199 (1998).
- [62] Y. Ralchenko, F.-C. Jou, D. Kelleher, A. Kramida, A. Musgrove, J. Reader, W. Wiese, and K. Olsen, *NIST Atomic Spectra Database Version 3.1.2* (2007), URL http://physics.nist.gov/cgi-bin/AtData/main_asd.
- [63] D. Goebel, U. Hohm, and G. Maroulis, *Phys. Rev. A* **54**, 1973 (1996).
- [64] H. A. Kurtz and K. D. Jordan, *J. Phys. B* **14**, 4361 (1981).
- [65] R. Szmtykowski, *J. Phys. II* **3**, 183 (1993).
- [66] G. F. Gribakin and W. A. King, *Can. J. Phys.* **74**, 449 (1996).
- [67] R. Campeanu, R. P. McEachran, L. A. Parcell, and A. D. Stauffer, *Nucl. Instrum. Methods Phys. Res. B* **143**, 21 (1998).
- [68] Y. Peng, C. Cheng, and Y. J. Zhou, *Chin. Phys. Lett.* **24**, 625 (2007).
- [69] T. S. Stein, M. Harte, J. Jiang, W. E. Kauppila, C. K. Kwan, H. Li, and S. Zhou, *Nucl. Instrum. Methods Phys. Res. B* **143**, 68 (1998).
- [70] T. S. Stein, J. Jiang, W. E. Kauppila, C. K. Kwan, H. Li, E. Surdutovich, and S. Zhou, *Can. J. Phys.* **74**, 313 (1996).
- [71] E. Surdutovich, M. Harte, W. E. Kauppila, C. K. Kwan,

- and T. S. Stein, Phys. Rev. A **68**, 022709 (2003).
- [72] N. I. Romanyak, O. B. Shpenik, A. I. Zhukov, and I. P. Zapesochnyi, Pis'ma. Zh. Tekh. Fiz. **6**, 877 (1980).
- [73] K. Bartschat, O. Zatsarinny, I. Bray, D. V. Fursa, and A. T. Stelbovics, J. Phys. B **37**, 2617 (2004).
- [74] O. Zatsarinny and K. Bartschat, Phys. Rev. A **71**, 022716 (2005).
- [75] P. D. Burrow, J. A. Michejda, and J. Comer, J. Phys. B **9**, 3225 (1976).
- [76] H. Nakanishi and D. M. Schrader, Phys. Rev. A **34**, 1810 (1986).
- [77] H. Nakanishi and D. M. Schrader, Phys. Rev. A **34**, 1823 (1986).
- [78] K. Strasburger, Struct. Chem. **15**, 415 (2004).
- [79] R. J. Buenker, H. Liebermann, M. Tachikawa, L. Pichl, and M. Kimura, Nucl. Instrum. Methods Phys. Res. B **247**, 47 (2006).
- [80] R. J. Buenker, H. Liebermann, L. Pichl, M. Tachikawa, and M. Kimura, J. Chem. Phys. **126**, 104305 (2007).